Research Square

Preprints are preliminary reports that have not undergone peer review.
They should not be considered conclusive, used to inform clinical practice,
or referenced by the media as validated information.

Differentiated Support of the West-Wing Auxiliary Haulage Roadway Passing through a Stopping-Line Coal Pillar

Yingfu Li
Anhui University of Science and Technology
Jiawei Yang
jiaweiyang_aust@163.com

Anhui University of Science and Technology
Shaoneng Du
China Coal Xinji Energy Co Ltd
Xun Zhang
China Coal Xinji Energy Co Ltd
Yuanfeng Fan
China Coal Xinji Energy Co Ltd
Guanfeng Chang
Anhui University of Science and Technology

Article

Keywords: stopping-line coal pillar, goaf, roadway surrounding rock, stress evolution, plastic zone, differentiated support design

Posted Date: July 20th, 2026

DOI: https://doi.org/10.21203/rs.3.rs-10292899/v1

License: This work is licensed under a Creative Commons Attribution 4.0 International License.
Read Full License

Additional Declarations: No competing interests reported.

Differentiated Support of the West-Wing Auxiliary Haulage Roadway Passing through a Stopping-Line Coal Pillar

Yingfu Li[1,2], Jiawei Yang[1*], Shaoneng Du[3], Xun Zhang[3], Yuanfeng Fan[3], Guanfeng Chang[4]

[1]School of Mining Engineering, Anhui University of Science and Technology, Huainan, 232001 Anhui China

[2]State Key Laboratory for Safe Mining of Deep Coal Resources and Environment Protection, Anhui University of Science and Technology, Huainan, 232000 Anhui China

[3]Banji Coal Mine,China Coal Xinji Energy Co Ltd, Bozhou, 236742 Anhui China

[4]School of Mechanics and Optoelectronic Physics, Anhui University of Science and Technology, Huainan, 232001 Anhui China.

[*]jiaweiyang_aust@163.com

ABSTRACT

To address the problems of non-uniform stress distribution, severe local plastic failure, and insufficient adaptability of uniform support in roadway surrounding rock under the combined mining influence of the stopping-line coal pillar and goaf, the west-wing auxiliary haulage roadway beneath the 110501 working face of Banji Coal Mine was taken as the engineering background. The floor failure depth after working face mining, the stress evolution characteristics of the underlying strata, and the deformation and failure characteristics of the roadway surrounding rock were investigated using theoretical analysis, numerical simulation, and field monitoring. Based on these results, a zonal differentiated support optimization scheme was proposed.The results show that after mining of the 110501 working face, the plastic failure depth of the floor is approximately 22 m, and the failure zone presents a bowl-shaped distribution. The shallow floor is dominated by tensile failure, whereas the deep floor gradually transforms into shear-slip failure. The vertical stress beneath the stopping-line coal pillar exhibits an obvious depth-dependent attenuation characteristic. A pressure-relief zone is formed beneath the goaf, while a high-stress concentration zone develops near the stopping-line coal pillar side.Along the excavation direction, the surrounding rock of the west-wing auxiliary haulage roadway shows significant zonal characteristics. In the coal-pillar influence zone, the peak vertical stress on the two ribs reaches 30.53 MPa, with a stress concentration factor of 1.74. Plastic failure is mainly concentrated in the two ribs, shoulder corners, and floor corners. According to the failure characteristics of the surrounding rock in the high-stress zone, an optimized support scheme was proposed by increasing the density of rib bolts, adding additional rib bolts, optimizing the symmetrical arrangement of cables, and increasing the cable length.Numerical simulation and field monitoring results indicate that after support optimization, the stress distribution in the roadway surrounding rock becomes more uniform, and the extent of the plastic zone is significantly reduced. The final roof-to-floor convergence and rib-to-rib convergence are reduced by 29.78% and 27.36%, respectively. The roof separation at the shallow and deep monitoring points is reduced by 15.22% and 6.15%, respectively. The research results can provide a reference for surrounding rock stability control and differentiated support design of deep roadways affected by stopping-line coal pillars.

Keywords： stopping-line coal pillar, goaf, roadway surrounding rock, stress evolution, plastic zone, differentiated support design

1. Introduction

With the continuous increase in coal mining depth and mining intensity, the disturbance range of mining-induced stress in coal and rock masses gradually extends into deeper strata, making the stability control of surrounding rock in deep roadways increasingly prominent. For underlying roadways located within the influence range of the overlying goaf and stopping-line coal pillar, the stability of the surrounding rock is controlled not only by the excavation disturbance of the roadway itself, but also by the combined effects of goaf pressure relief, concentrated loading from the coal pillar, and stress transfer through the floor after overlying coal seam mining.As an important load-bearing structure remaining after the completion of working face extraction, the stopping-line coal pillar can alter the original stress distribution in the underlying strata, resulting in the formation of a high-stress concentration zone beneath the coal pillar and a relatively pressure-relieved zone beneath the goaf. Under such a non-uniform stress environment, the roadway often exhibits pronounced zonal loading and differentiated failure characteristics along the excavation direction. Consequently, conventional uniform support parameters are difficult to fully satisfy the requirements for surrounding rock stability control in different roadway sections.Therefore, investigating the stress evolution characteristics and differentiated support method for the surrounding rock of underlying rock roadways under the combined influence of the stopping-line coal pillar and goaf is of great significance for ensuring the long-term stability of deep development roadways.

Deep roadway surrounding rock control under complex geological and mining conditions has long been an important research topic in the field of safe coal mining. Kang [1] systematically summarized the development of support technologies for deep and complex coal roadways, and pointed out that high in situ stress, strong mining-induced disturbance, and complex surrounding rock structures are the main factors affecting roadway stability. Xie et al. [2] analyzed the surrounding rock control mechanism from the perspective of the evolution of the load-bearing structure in deep coal roadways, and suggested that the support structure should work synergistically with the load-bearing ring of the surrounding rock to improve the overall roadway stability. Wang et al. [3] investigated the deformation of the surrounding rock and the stress evolution of the coal pillar in a pre-driven withdrawal roadway during the final mining stage of a working face, and showed that coal-pillar stress concentration and roof movement significantly affect roadway surrounding rock deformation. These studies indicate that, under deep mining-induced disturbance, roadway surrounding rock stability is closely related to mining-induced stress redistribution, evolution of the surrounding rock load-bearing structure, and adaptability of the support system.

The concentrated load induced by stopping-line coal pillars and residual coal pillars is an important factor controlling the stress distribution of underlying strata and roadway stability. Kang et al. [4] investigated the attenuation law of concentrated stress transferred from coal pillars in close-distance coal seams to the underlying strata, and pointed out that the concentrated stress beneath the coal pillar gradually decreases with increasing distance from the coal pillar and increasing floor depth, although an obvious stress gradient still exists near the coal-pillar boundary. Liu et al. [5] studied the instability mechanism of roadways under the condition of retained coal pillars in close-distance coal seams, and concluded that stress concentration and plastic failure of surrounding rock in the coal-pillar influence zone are important causes of intensified roadway deformation. Wang et al. [6] investigated the optimization mechanism of lower return-air roadway layout under the influence of residual coal pillars, and indicated that overlying residual coal pillars significantly change the stress state and plastic zone distribution of the surrounding rock of lower roadways. Wu et al. [7] analyzed the stress field and damage evolution of coal and rock masses in residual coal pillar zones after slicing mining of thick coal seams, and suggested that stress concentration zones and damage development zones are prone to form beneath residual coal pillars. Wang et al. [8] further revealed the deformation and failure mechanism of lower roadways in close-distance residual coal pillar zones, showing that roadway surrounding rock failure under the influence of residual coal pillars is characterized by obvious non-uniformity and local concentration. These findings provide an important basis for analyzing stress transfer beneath stopping-line coal pillars and roadway surrounding rock failure.

The floor failure depth beneath the goaf is a key parameter for determining the reasonable layout horizon of underlying roadways and evaluating the influence range of mining-induced disturbance. After working face extraction, overburden movement and abutment pressure transfer lead to reconstruction of the original stress field in the floor strata, thereby inducing tensile failure, shear-slip failure, and expansion of the plastic zone in the floor. Li et al. [9] investigated the floor failure mechanism under repeated mining of close-distance coal seams through mechanical analysis, and found that mining-induced stress redistribution causes deformation and failure of the floor strata. Liu et al. [10] predicted coal seam floor failure depth using a zoning method for shallow and deep mining conditions, and pointed out that mining depth, mining height, working face size, and mechanical parameters of coal and rock masses all affect the development degree of floor failure. Kong et al. [11] established a plastic slip failure model for the floor of multiple composite coal seams, and analyzed floor failure depth and failure morphology through numerical simulation. Related studies show that floor failure exhibits obvious zonation and progressive development. The shallow floor is prone to tensile failure under goaf pressure relief, whereas the deep floor is more strongly controlled by concentrated abutment pressure and mainly undergoes shear-slip failure. Therefore, when determining the layout horizon of underlying rock roadways, floor failure depth, coal-pillar stress transfer, and the pressure-relief range of the goaf should be comprehensively considered.

Under the combined influence of the goaf and residual coal pillars, the failure of surrounding rock in underlying roadways usually exhibits obvious spatial differences. Yin et al. [12] investigated the non-uniform failure of roadways beneath irregular goafs, and pointed out that the combined action of residual coal pillars and goafs can lead to differentiated and asymmetric failure at different roadway positions, based on which zonal control technology was proposed. Wang et al. [13] studied the stability control of gob-side entry driving beneath staggered residual coal pillars in close-distance coal seams, and showed that residual coal-pillar loading and goaf stress recovery jointly affect the stress distribution and deformation characteristics of underlying roadways. Xia et al. [14] investigated the stability of roadways with small coal pillars under repeated mining through numerical simulation, and indicated that repeated mining promotes the expansion of plastic zones in coal pillars and surrounding rock. Shang et al. [15] studied the failure characteristics and control technology of roadway surrounding rock under repeated mining of close-distance coal seams, and found that the stress, fractures, and plastic zones of roadway surrounding rock all exhibit obvious staged and regional characteristics. These studies suggest that, under the combined mining influence of the stopping-line coal pillar and goaf, the underlying roadway may successively pass through the coal-pillar high-stress influence zone, the stopping-line stress transition zone, and the goaf pressure-relief zone along the excavation direction, with significant differences in surrounding rock stress level, plastic zone extent, and dominant failure positions among different sections.

Bolt–cable combined support is the main technical approach for surrounding rock control in coal mine roadways, but its control effect depends on the matching degree between support parameters and the loading state and failure characteristics of the surrounding rock. Xiang et al. [16] investigated the failure characteristics of bolt support and stability control technology for roadways in thick coal seams, and pointed out that bolt and cable support parameters should be optimized according to the failure range and main deformation positions of the surrounding rock. Xie et al. [17] proposed a control technology for the deformation mechanism of weak coal roadways under high horizontal stress, and considered that improving the confinement capacity of shallow surrounding rock and enhancing the stability of the deep load-bearing structure are key to controlling roadway deformation. Yao et al. [18] studied the instability mechanism and surrounding rock control technology of roadways under dynamic loading induced by short-distance mining, and indicated that support strength and support timeliness should be improved under the superposition of dynamic and static loads. Chen et al. [19] proposed a zonal differentiated control method for mining roadways beneath residual coal pillars in close-distance coal seams, demonstrating that targeted reinforcement support in the strong coal-pillar influence zone can effectively improve surrounding rock stability. Li et al. [20] studied the optimization of lower coal seam roadway layout under the influence of coal-pillar stress transfer, further confirming the important influence of coal-pillar

concentrated loading on underlying roadway layout and support design. These studies show that, when the surrounding rock stress environment and failure positions exhibit obvious zonal differences, differentiated support is more conducive to matching support strength with surrounding rock control requirements.

In summary, existing studies have achieved substantial progress in deep roadway support, residual coal-pillar stress transfer, stability of roadways beneath goafs, floor failure depth, and optimization of bolt–cable support. However, research on the stability control of deep rock main roadways under the combined influence of stopping-line coal pillars and goafs remains insufficient. First, the relationship between floor failure depth after working face mining and the reasonable layout horizon of underlying rock roadways has not been systematically analyzed. Second, the coupling mechanism between the vertical stress attenuation law at different depths beneath the stopping-line coal pillar and the goaf pressure-relief effect is still not well understood. Third, few studies have examined the zonal characteristics of surrounding rock stress, plastic zones, and deformation failure during the transition from the coal-pillar high-stress zone to the goaf pressure-relief zone along the roadway excavation direction. Fourth, existing support schemes mostly adopt uniform support parameters, which are difficult to adapt to the differences in surrounding rock stress environments and failure positions among different roadway sections. Therefore, it is necessary to carry out surrounding rock stability evaluation and zonal differentiated support research for underlying rock roadways affected by stopping-line coal pillars. Taking the west-wing auxiliary haulage roadway beneath the 110501 working face of Banji Coal Mine as the engineering background, this study investigates the problems of non-uniform stress distribution, severe local plastic failure, and insufficient adaptability of uniform support in roadway surrounding rock under the combined mining influence of the stopping-line coal pillar and goaf. The study is conducted using theoretical analysis, FLAC3D numerical simulation, and field monitoring. The research results can provide a reference for reasonable layout, surrounding rock stability evaluation, and zonal differentiated support design of deep rock roadways affected by stopping-line coal pillars.

2. Engineering Overview

Banji Coal Mine is located at the junction of Lixin County and Yingshang County, Fuyang City, Anhui Province. The main minable coal seams of the mine are the No. 8, No. 5, and No. 1 coal seams. The 110501 working face has a strike length of 835 m and an inclined length of 281 m. It adopts a strike longwall mining layout, with fully mechanized full-seam mining in a single slice, and the roof is managed by the full-caving method.

The 110501 working face is located in the No. 5 coal seam of the 1105(8) mining district. The thickness of the No. 5 coal seam in the main mining area ranges from 3.37 m to 6.95 m, with an average thickness of 5.67 m, indicating a medium-thick to thick coal seam. The ground elevation ranges from +24.67 m to +26.58 m, while the elevation of the No. 5 coal seam floor ranges from -711.2 m at the highest point to -774.3 m at the lowest point. The dip angle of the coal seam varies from 0° to 10°, with an average dip angle of 6°.

To ensure stable mine production continuity, it is necessary to develop and prepare the west-wing mining district as early as possible, and to excavate the west-wing main development roadways after the goaf of the 110501 working face has stabilized. The west-wing auxiliary haulage roadway is located beneath the 110501 working face and is arranged in the floor strata of the No. 5 coal seam. To ensure the stability of roadway support, the reasonable location of the west-wing auxiliary haulage roadway should be determined. The designed positions of the 110501 working face and the west-wing auxiliary haulage roadway are shown in Fig. 1.

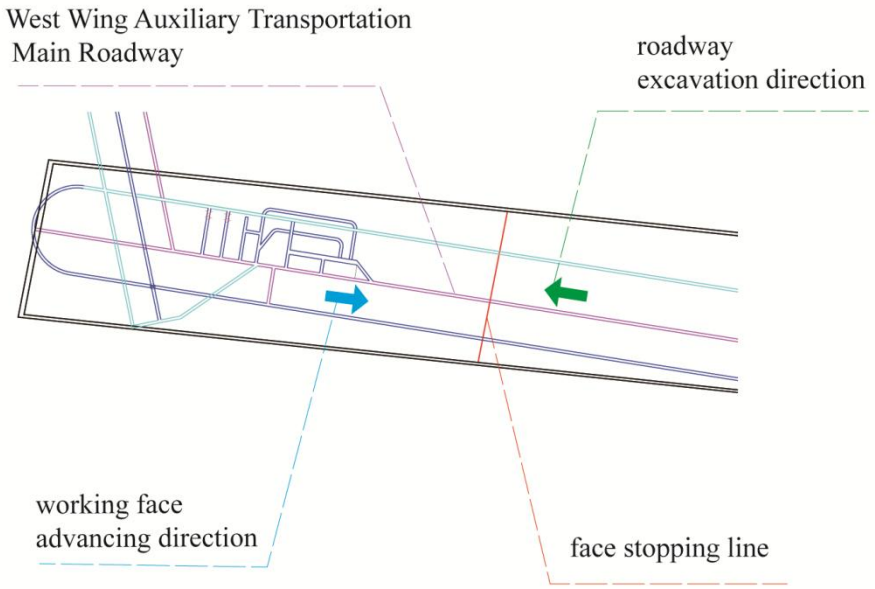


Figure 1. Layout of the Working Face and the West-Wing Auxiliary Haulage Roadway.

3. Floor Failure Characteristics Induced by Coal Seam Mining at the Working Face

After the completion of mining at the 110501 working face, the mining-induced stress was gradually transferred into the deeper floor strata, resulting in the redistribution of the original floor stress field and inducing deformation and failure of the floor rock strata. Based on the plastic slip-line field theory, the floor failure of the stope can be regarded as a plane-strain plastic failure problem of a semi-infinite body subjected to abutment pressure. According to the distribution characteristics of the slip-line field, the floor failure zone can be divided into active zone I, transition zone II, and passive zone III, as shown in Fig. 2. Among them, the active zone is the initial region of plastic yielding in the floor; the transition zone consists of logarithmic spiral slip lines and mainly serves to transfer stress and coordinate deformation; and the passive zone is located at the outer margin of the plastic zone, providing confinement and equilibrium.

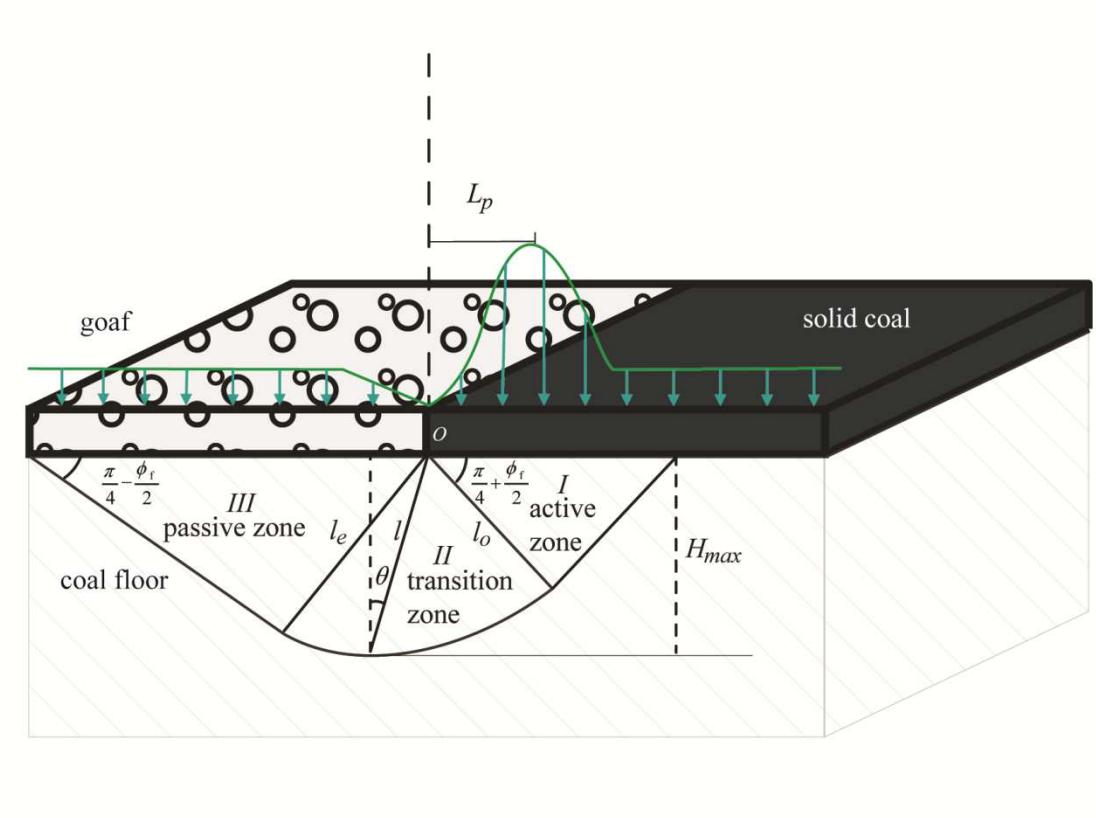


Figure 2. Mechanical Model of the Floor Failure Zone.

For active stress zone I, according to the geometric relationship of the active zone, the initial radius of the logarithmic spiral slip line in the transition zone is expressed as:

$$l_o = \frac{L_p}{2\cos\left(\frac{\pi}{4}+\frac{\varphi_f}{2}\right)} \tag{1}$$

where l_o is the initial radius of the logarithmic spiral slip line, and L_p is the width of the plastic zone in front of the coal wall. The slip line in the transition zone follows the logarithmic spiral equation:

$$l(\theta) = l_o e^{\theta \tan\varphi_f} \tag{2}$$

where θ is the polar angle measured from the boundary of the active zone, with a value range of $0 \leqslant \theta \leqslant \pi/4+\varphi_f/2$. According to the geometric relationship of the slip-line field, the vertical failure depth of any point in the transition zone relative to the horizontal plane of the floor can be expressed as:

$$h(\theta) = l_o e^{\theta \tan\varphi_f} \cos\left(\theta-\frac{\pi}{4}+\frac{\varphi_f}{2}\right) \tag{3}$$

where $h(\theta)$ is the floor failure depth corresponding to the polar angle (\theta). By determining the extremum of Eq. (3), the polar angle corresponding to the maximum failure depth can be obtained as:

$$\theta_{\max} = \frac{\pi}{4}+\frac{\varphi_f}{2} \tag{4}$$

Substituting Eq. (4) into Eq. (3) and combining with Eq. (2), the maximum floor failure depth in the goaf of the 110501 working face is given by:

$$H_{\max} = \frac{L_p \cos\varphi_f}{2\cos\left(\frac{\pi}{4}+\frac{\varphi_f}{2}\right)} e^{\left(\frac{\pi}{4}+\frac{\varphi_f}{2}\right)\tan\varphi_f} \tag{5}$$

where $\boldsymbol{H_{max}}$ is the maximum floor failure depth, m; $\boldsymbol{L_p}$ is the width of the plastic zone in front of the coal wall, m; and $\boldsymbol{\varphi_f}$ is the internal friction angle of the floor rock mass, °.

Based on the limit equilibrium theory, an infinitesimal element within the plastic zone ahead of the coal wall is selected for force analysis, and the coal mass is assumed to satisfy the Mohr-Coulomb yield criterion. Considering the strength parameters of the coal mass, the frictional effect at the coal-roof and coal-floor interfaces, and the abutment pressure concentration effect, the width of the plastic zone ahead of the coal wall can be obtained as:

$$L_p = \frac{M}{2\xi f}\ln\left[\frac{K\gamma H + C_c\cot\varphi_c}{\xi C_c\cot\varphi_c}\right] \tag{6}$$

where $\boldsymbol{M}$ is the mining height of the working face, m; $\boldsymbol{f}$ is the friction coefficient at the interfaces between the coal seam and the roof and floor strata; $\boldsymbol{\xi}$ is the triaxial stress coefficient, $\xi = \frac{1+\sin\varphi_c}{1-\sin\varphi_c}$; $\boldsymbol{K}$ is the abutment pressure concentration factor; $\boldsymbol{\gamma}$ is the average unit weight of the overlying strata, taken as (25kN/m^3); $\boldsymbol{H}$ is the burial depth of the working face, m; $\boldsymbol{C_c}$ is the cohesion of the coal mass, MPa; and $\boldsymbol{\varphi_c}$ is the internal friction angle of the coal mass, °.

By substituting Eq. (6) into Eq. (5), the following expression can be obtained:

$$H_{\max} = \frac{M\cos\varphi_f}{4\xi f\cos\left(\frac{\pi}{4}+\frac{\varphi_f}{2}\right)}\ln\left[\frac{K\gamma H + C_c\cot\varphi_c}{\xi\left(p_1 + C_c\cot\varphi_c\right)}\right] e^{\left(\frac{\pi}{4}+\frac{\varphi_f}{2}\right)\tan\varphi_f} \tag{7}$$

To further analyze the influence of coal seam occurrence characteristics and mining technology on the floor failure depth, Fig. 3 shows that, under otherwise unchanged conditions, the floor failure depth exhibits a more significant response to the mining height in terms of the contour distribution pattern. As the mining height increases, the contours change more rapidly in the horizontal direction, indicating that mining height is the dominant factor controlling the development of floor failure depth. An increase in mining height significantly enlarges the width of the plastic zone ahead of the coal wall, thereby causing the slip-induced floor failure zone to extend deeper into the floor strata.

With increasing burial depth, the self-weight stress of the overlying strata increases, and the abutment pressure ahead of the coal wall is enhanced. As a result, the plastic zone in the coal mass further expands and is transmitted to the deeper floor strata through the slip-line field, leading to an increase in the floor failure depth. However, compared with mining height, burial depth mainly affects the width of the plastic zone ahead of the coal wall through the logarithmic term; therefore, its influence is relatively moderate.

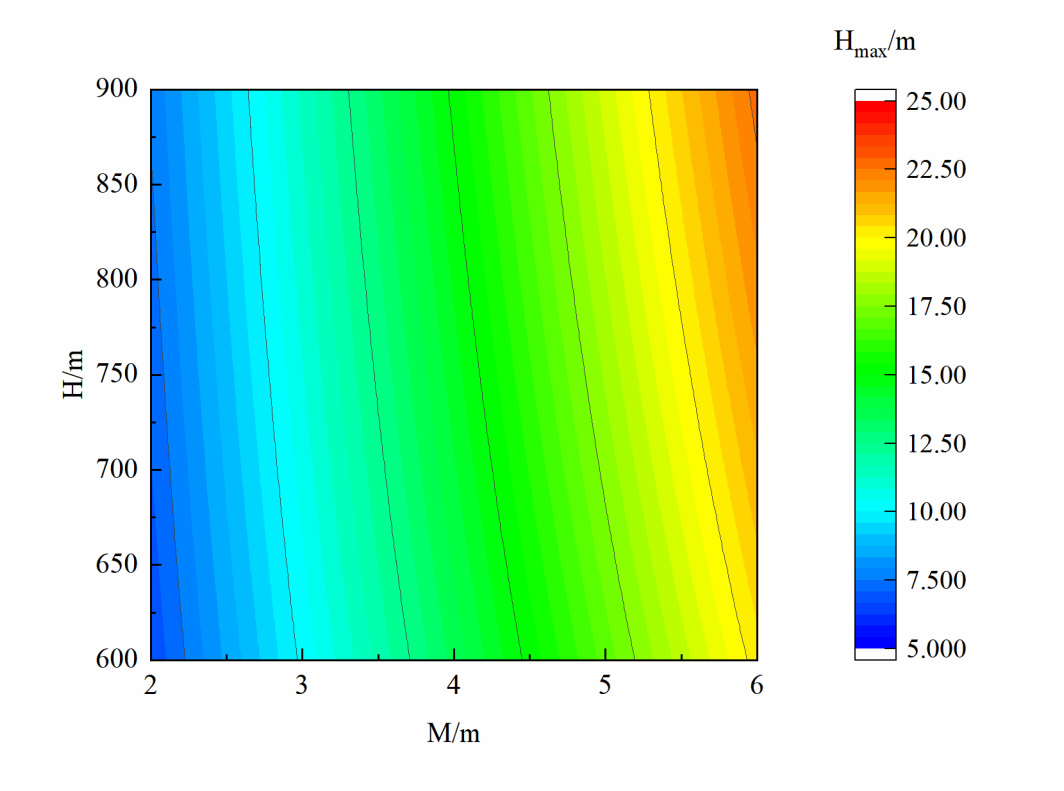


Figure 3. Effects of Mining Height and Burial Depth on Floor Failure Depth.

According to the in situ measurement results of the working face and the laboratory mechanical test results of the coal and rock masses, the actual mechanical parameters of the rock mass at the working face were determined, as listed in Table 1.

Parameters	Value
M/m	6
f	0.3
K	1.88
H/m	800
γ/(kN/m^3)	25
φ_f/°	29
C_c/MPa	0.21
φ_c/°	25

Table 1. Parameters of the Coal and Rock Masses

By substituting the in situ rock mass parameters into Eq. (7), the maximum floor failure depth induced by mining of the 110501 working face was calculated to be H_{max}=21.98m. This result indicates that the mining-induced stress can be transferred into the deeper floor strata, and that the floor rock mass has a significant risk of plastic failure.

4. Numerical Simulation of Surrounding Rock Stability

4.1 Establishment of the Numerical Calculation Model

According to the in situ rock mechanical parameters of the strata at Banji Coal Mine, a numerical model was established using FLAC3D numerical simulation software to analyze the

evolution characteristics of the surrounding rock of the underlying roadway, namely the west-wing auxiliary haulage roadway, under the influence of the 110501 goaf. The mechanical parameters of the coal and rock masses are listed in Table 2.

The model dimensions, namely length × width × height, are 420 m × 340 m × 170 m. The Mohr-Coulomb constitutive model was adopted. The length of the goaf was set to 100 m. To avoid boundary effects, 80 m-wide protective coal pillars were retained on all four sides of the model. Displacement constraints were applied to the bottom and lateral boundaries of the model to restrict movement. The entire model consisted of 1,693,000 zones and 1,737,705 grid points. To ensure the calculation accuracy of the model, local mesh refinement was conducted for the surrounding rock near the roadway. The numerical calculation model is shown in Fig. 4.

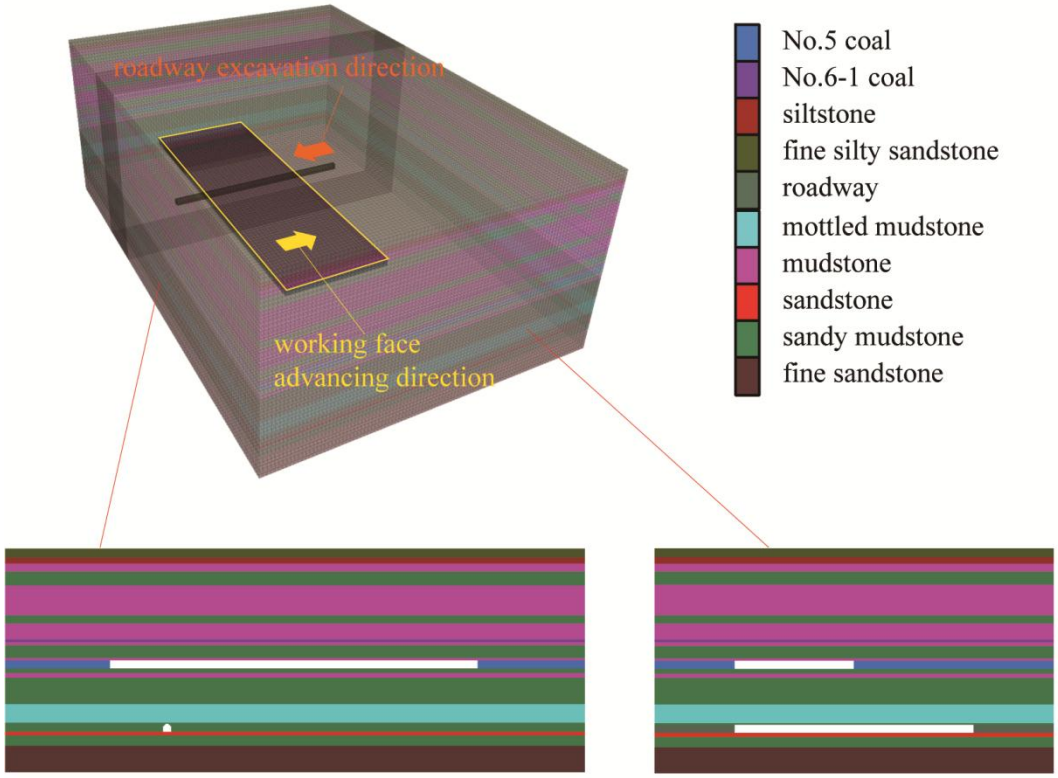


Figure 4. Numerical Calculation Model.

Rock Layer	Density (kg/m^3)	Elastic modulus (GPa)	Poisson's ratio	Internal friction angle(°)	Cohesion (MPa)
Fine Silty Sandstone	2650	10.2	0.22	36.6	3.8
Siltstone	2586	12.5	0.27	33.54	3.2
No. 6-1 Coal	1465	2.02	0.31	25.1	0.22
No. 5 Coal	1470	2.02	0.32	25.0	0.21
Sandy Mudstone	2627	22.14	0.27	29.0	2.00
Mudstone	2480	5.2	0.3	28	1.85
Mottled Mudstone	2400	4.8	0.3	27	1.6
Sandstone	2686	25.0	0.2	33.54	2.76
Fine Sandstone	2650	12.8	0.25	38.2	4.5

Table 2. Physical and Mechanical Parameters of Rock Strata

4.2 Evolution Characteristics of the Surrounding Rock in the Underlying Strata of the 110501 Working Face

Fig. 5 illustrates the plastic yielding characteristics of the floor strata beneath the goaf of the 110501 working face. The simulation results indicate that mining of the 110501 working face induces plastic yielding within approximately 22 m of the floor strata, which agrees well with the theoretical calculation. As shown in the figure, the plastic zone in the floor generally presents a semi-ellipsoidal or bowl-shaped failure pattern centered beneath the goaf, exhibiting distinct zonation and progressive evolution with increasing depth.

In the shallow floor strata directly beneath the goaf, large-scale unloading leads to a pronounced release of horizontal stress, thereby inducing severe floor heave and tensile failure. In the middle floor strata, the surrounding rock is subjected to the combined effects of tensile and shear stresses, forming a tensile-shear composite failure zone. In contrast, in the deeper and marginal regions of the floor, the surrounding rock is mainly affected by concentrated abutment pressure transferred from the overlying strata, and the dominant failure mode gradually changes from tensile failure in the shallow strata to shear-slip instability in the deep strata.

Overall, floor failure beneath the goaf is a progressive process characterized by the transition from shallow tensile failure to deep shear failure. The final maximum failure depth is primarily governed by the shear strength of the floor rock mass, while the shallow floor heave caused by goaf unloading and the associated tensile failure are the fundamental driving mechanisms of the floor failure process.



Figure 5. Distribution of the Plastic Zone in the Strata Beneath the Goaf of the 110501 Working Face.

Fig. 6 presents the vertical stress contours of the 110501 working face at different advancing distances. During face advancement, the influence of upper coal seam mining on the underlying strata beneath the No. 5 coal seam is mainly manifested as a stress redistribution pattern characterized by pressure relief in the central goaf region and stress concentration on both sides. With increasing advancing distance, the pressure-relief zone gradually expands, whereas the high-stress concentration zone progressively migrates toward

the goaf boundary and the coal pillar side. The maximum vertical stress increases from 24.940 MPa to 34.596 MPa, corresponding to an increase of approximately 38.7%.

These results indicate that the influence of overlying mining on the roadway beneath the No. 5 coal seam is spatially heterogeneous rather than uniformly distributed. The strata beneath the central goaf generally remain in a relatively pressure-relieved state, while high stress concentration is prone to occur near the goaf boundary, the coal pillar edge, and the stopping-line-affected zone. Therefore, these high-stress regions should be regarded as the key zones for surrounding rock deformation control and zonal reinforcement support design.

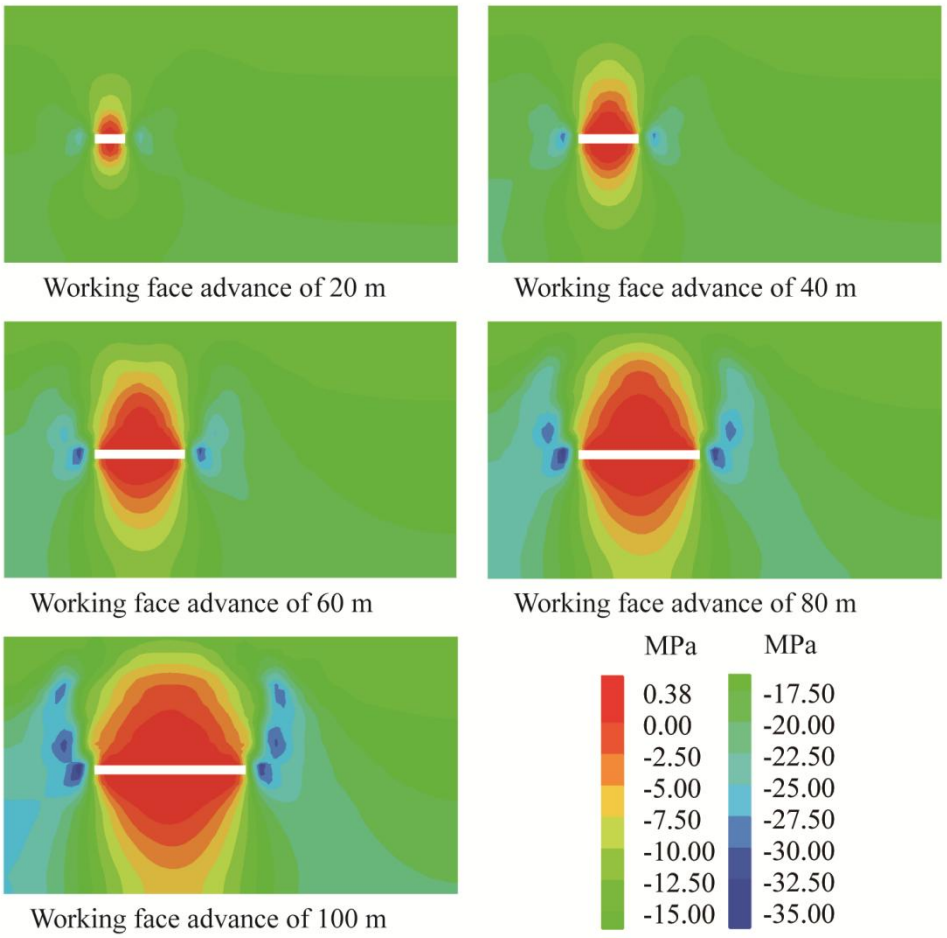


Figure 6. Vertical Stress Distribution Contours at Different Advancing Distances of the Working Face.

To further reveal the stress distribution characteristics of the stopping-line coal pillar, the longitudinal section at a face advance distance of 100 m was selected as a representative section, and the vertical stress distribution curves of the underlying rock strata at different depths were obtained. Fig. 7 presents the vertical stress distribution curves of the strata located 10 m, 20 m, 30 m, and 40 m below the floor along the longitudinal section at the roadway position of the stopping line in the 110501 working face of the No. 5 coal seam. As shown in the figure, after mining of the 110501 working face, the stopping-line coal pillar induces a distinctly non-uniform stress distribution in the coal seam floor. Specifically, the vertical stress in the floor exhibits a typical mining-induced abutment pressure pattern, characterized by stress concentration on the solid coal side and stress relief on the goaf side.

As the section approaches the stopping line from the deep solid coal side, the vertical stress at all investigated depths increases progressively and forms a peak corresponding to the advanced abutment pressure. The shallower the floor depth, the higher the stress peak. In particular, the peak stress in the shallow rock stratum at 10 m below the No. 5 coal seam floor is about 25 MPa. As the depth increases to 20 m, 30 m, and 40 m, the peak stress decreases successively, indicating that the advanced concentrated stress undergoes diffusion

and dissipation as it is transferred into the deeper floor strata. Meanwhile, with increasing floor depth, the position of the stress peak gradually shifts toward the deeper solid coal side. The stress peak in the shallow strata is located closer to the stopping line, whereas the high-stress zone in the deep strata migrates outward. In addition, the variation gradient of stress in the deep strata becomes more gradual, indicating that the intensity of mining disturbance decreases significantly with increasing floor depth. In the transition zone near the stopping line (x=0), the vertical stress at all depths continuously decreases after passing the peak value, and by the stopping-line position it has dropped substantially below the peak level. The stress reduction in the shallow strata is much greater than that in the deep strata, suggesting that the shallow floor is more sensitive to mining disturbance from the coal wall of the working face.

After entering the goaf, the vertical stress in the floor shows a rapid attenuation trend, continuously decreasing with increasing distance from the stopping line and eventually approaching a stable low-stress state, thereby forming a large-scale pressure-relief zone in the floor. At the same horizontal distance, the greater the floor depth, the higher the vertical stress value, indicating that the pressure-relief effect gradually weakens with increasing depth. Therefore, the degree and extent of mining-induced stress disturbance in the floor strata exhibit a pronounced depth-dependent effect: the shallow floor is more strongly affected by the advanced abutment pressure and shows a more obvious pressure-relief effect beneath the goaf, whereas the deep floor experiences weaker stress concentration and a smoother stress distribution. To ensure roadway stability and support performance, the west-wing auxiliary haulage roadway is arranged in the sandstone stratum located 40 m below the floor of the goaf of the 110501 working face.

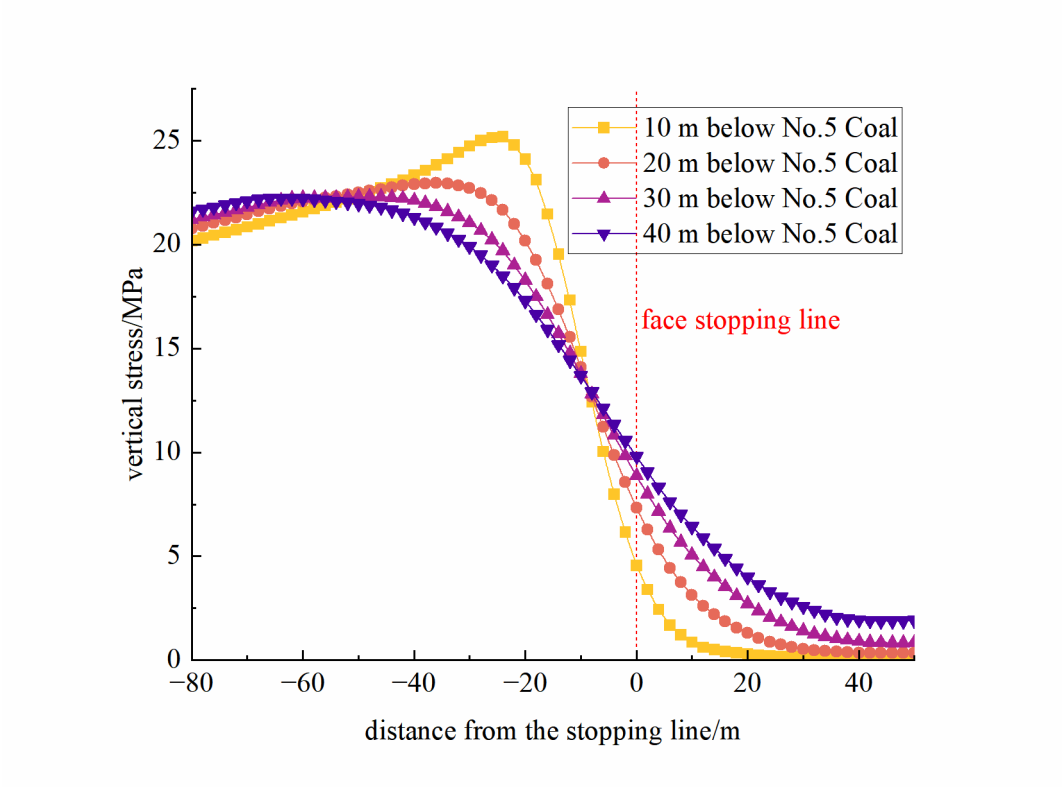


Figure 7. Vertical Stress Distribution Curves at Different Depths.

4.3 Stress Evolution Characteristics of the Surrounding Rock of the West-Wing Auxiliary Haulage Roadway

As shown in Fig. 8, the vertical stress of the roadway surrounding rock exhibits a pronounced zonal distribution. Taking the stopping line as the boundary, the roadway can be divided into the overlying coal-pillar influence zone and the pressure-relief influence zone beneath the goaf overburden. The vertical stress at all monitoring points around the roadway

shows an evolutionary pattern characterized by initial stability followed by a gradual decrease.

Within the range of -80 to 0 m, which is under the influence of the coal-pillar overburden, the surrounding rock on both sides of the roadway is generally in a high-stress concentration state. In particular, the section from -80 m to -40 m from the stopping line corresponds to the core influence zone of coal-pillar abutment pressure. In this zone, the peak vertical stress on the two ribs of the roadway reaches 30.53 MPa, and the stress concentration factor of the surrounding rock is 1.74, indicating a significant lateral transfer effect of coal-pillar abutment pressure and a pronounced high-stress concentration on the roadway ribs. The stress values at all monitoring points remain relatively stable in this section.In the transitional section from -40 m to 0 m from the stopping line, the vertical stress at all monitoring points begins to show a marked decreasing trend. The vertical stress on both ribs of the roadway gradually decreases from 27 MPa to 15 MPa, indicating that the surrounding rock of the roadway is transitioning from a high-stress concentration zone to a pressure-relief zone, with a significant stress release effect in this section. Meanwhile, the stress gradient changes considerably in this interval, and the mechanical state of the surrounding rock transforms from a high-stress bearing state to a relaxed state after mining-induced pressure relief.After crossing the stopping line, the roadway enters the pressure-relief zone beneath the goaf overburden, where the vertical stress in the surrounding rock at all monitoring points decreases sharply. Within the range of 20-40 m from the stopping line, the stresses on the two ribs decrease to approximately 4-5 MPa, the stresses at the left and right shoulders decrease to about 2-3 MPa, and the roof stress decreases to about 1-2 MPa, all reaching very low levels.

Within the stress concentration zone, the stress values on the two ribs of the roadway (left rib and right rib) are the highest, both remaining at around 30 MPa; the stresses at the left and right shoulders are about 20-23 MPa; and the roof stress is the lowest, at approximately 8 MPa. The degree of stress concentration on the two ribs is significantly higher than that at the roof and shoulders, and a distinct pressure-relief zone exists behind the stopping line, where the stress attenuation exceeds 80%. This reflects the mechanical response process in which the surrounding rock stress near the stopping line transfers from a high abutment-pressure state to a low-stress state. In addition, the stress distribution on the two roadway ribs shows good symmetry. The vertical stress contours of the roadway are shown in Fig. 9.

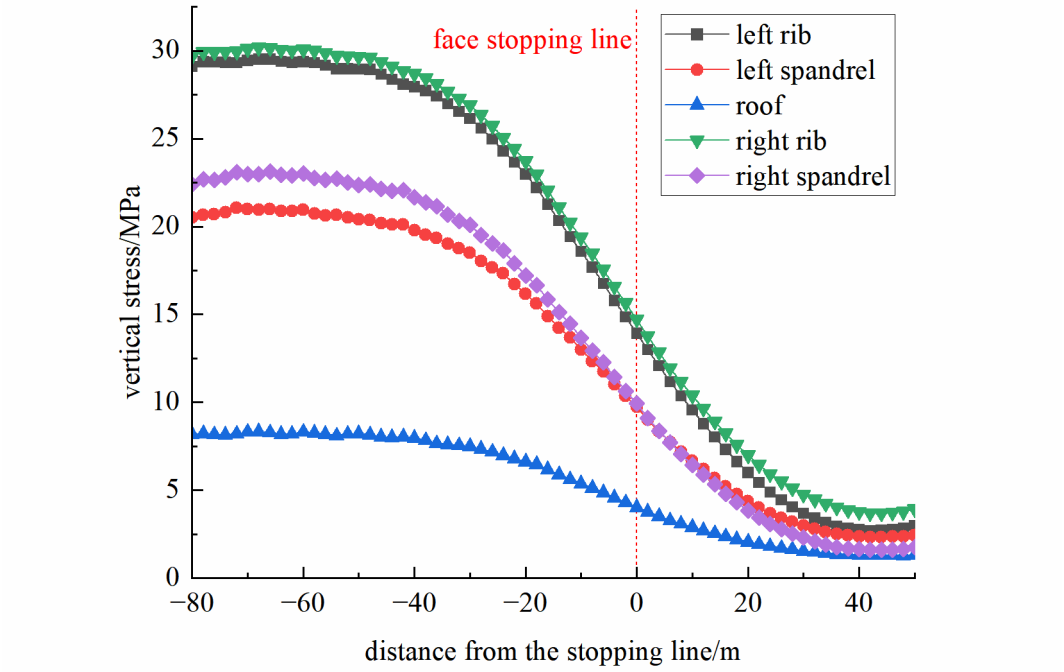


Figure 8. Vertical Stress Curves of the Roadway.

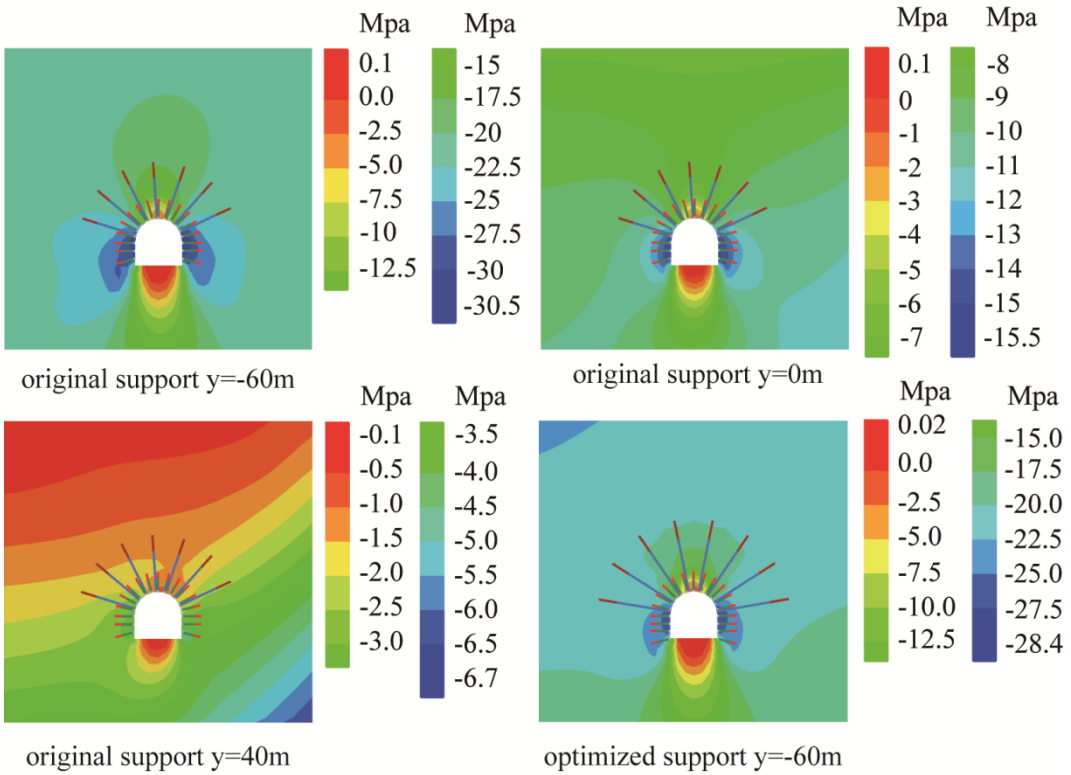


Figure 9. Comparison of Vertical Stress in the West-Wing Auxiliary Haulage Roadway.

4.4 Evolution Characteristics of the Plastic Zone in the Surrounding Rock of the West-Wing Auxiliary Haulage Roadway

The plastic zone of the roadway is shown in Fig. 10. Along the roadway axis, the development patterns of the surrounding rock plastic zone differ significantly among different sections. Failure is mainly concentrated in the roof shoulder corners, the two ribs, and the floor corners, whereas the plastic zone directly above the arch crown is relatively weak, indicating that under the original support conditions, the surrounding rock failure exhibits pronounced positional heterogeneity.

At the section beneath the coal pillar (y=-60m), the plastic zone reaches its maximum extent and exhibits a continuous failure pattern from the ribs to the shoulder corners and then to the floor corners. The two ribs and floor corners show both a history of shear yielding and locally sustained shear failure, while the floor corners and the shallow floor strata exhibit tensile-shear composite failure. The plastic zone is extensively developed, indicating that the concentrated stress disturbance induced by the coal pillar is strong and that the original support provides insufficient confinement for the ribs and floor corners.At the section beneath the stopping line (y=0m), the plastic zone remains concentrated in the two ribs, shoulder corners, and floor corners, but its extent is reduced compared with that beneath the coal pillar. Distinct shallow shear plastic zones are still observed in the two ribs. Owing to the combined effects of the coal-pillar boundary and goaf pressure relief, stress redistribution in this section is relatively complex, and the tendency for local shear failure remains strong.At the section beneath the goaf (y=40m), the plastic zone contracts further and is mainly confined to the vicinity of the two ribs and floor corners, while plastic failure in the roof and shoulder corners is significantly weakened. At this section, the plastic response is dominated by historical shear yielding, and the degree of ongoing shear failure is markedly lower than that at the previous two sections. This is attributed to the pressure-relief effect of overlying mining beneath the goaf, which reduces both the stress concentration level and the loading intensity acting on the surrounding rock.

From the section beneath the coal pillar to those beneath the stopping line and the goaf, the scale of the surrounding rock plastic zone shows a decreasing trend, and the degree of failure can be ranked as follows: beneath the coal pillar > beneath the stopping line > beneath the goaf. The dominant failure mode is shear failure, while tensile-shear composite failure locally occurs in the floor corners and shallow floor strata. Under the original support conditions, the overall stability of the roof is relatively good; however, in the coal-pillar zone and the stopping-line influence zone, the plastic zones in the two ribs, shoulder corners, and floor corners are extensive, with local sustained shear failure still occurring. This indicates that the original support scheme is unable to adapt to the differences in surrounding rock deformation and failure under varying stress environments.

Therefore, subsequent support optimization should focus on strengthening support in the aforementioned zones, increasing the density of bolts and cables in the ribs, and enhancing the confinement capacity of the floor corners, so as to suppress further expansion of the plastic zone and improve the stability of the overall load-bearing structure of the surrounding rock.

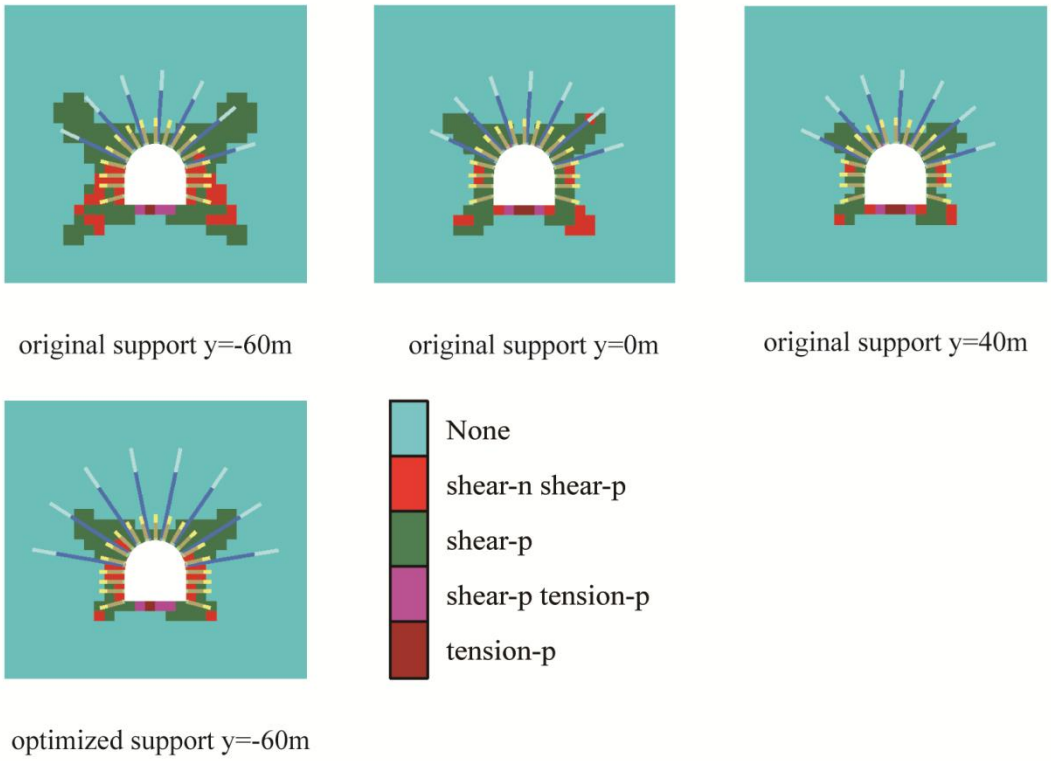


Figure 10. Comparison of the Plastic Zone in the West-Wing Auxiliary Haulage Roadway.

4.5 Optimized Support Design for the West-Wing Auxiliary Haulage Roadway

The stability of the surrounding rock of the west-wing auxiliary haulage roadway is jointly affected by stress concentration induced by the stopping-line coal pillar and roadway excavation disturbance, with the stress concentration effect of the coal pillar being the most significant. Considering the long service life of the west-wing auxiliary haulage roadway, the stability of different stress zones of the roadway under the influence of the stopping-line coal pillar of the 110501 working face was investigated. Based on the engineering conditions of Banji Coal Mine and the differentiated stress characteristics in different roadway zones, a zonal control support scheme was proposed using primary support as the design principle. According to the vertical stress distribution and plastic zone evolution of the surrounding rock, a differentiated surrounding rock control scheme should be adopted in the stress concentration zone, located approximately −80 to −40 m from the stopping line, to ensure the long-term stability of the roadway.

The west-wing auxiliary haulage roadway has a width of 6.0 m, a height of 5.0 m, and a net cross-sectional area of 26.1 m^2. The original support scheme adopted the same support

pattern in all roadway sections. This original support scheme shows good applicability in the pressure-relief zone beneath the goaf and in low-disturbance zones far from the concentrated influence of the stopping-line coal pillar. The original support adopts a combined bolt–mesh–cable–shotcrete support system. The support materials include metal meshes with specifications of Φ6 mm@100 mm × 60 mm and Φ6 mm@100 mm × 100 mm, as well as H-type steel strips and M5 steel strips. The bolts are Φ22 mm × 2500 mm left-hand threaded high-strength steel bolts, with a spacing and row spacing of 800 mm × 800 mm. The cables are 1×19S-21.8-1860 steel strands with a length of 7200 mm, and the spacing and row spacing are 1200 mm × 1200 mm. The support cross-section is shown in Fig. 11.

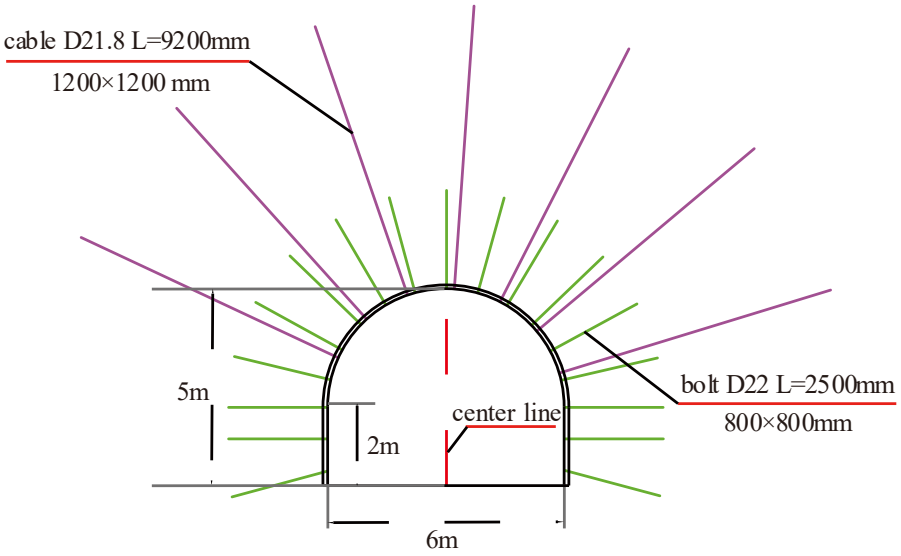


Figure 11. Cross-Section of the Original Roadway Support.

According to the evolution characteristics of the plastic zone under the original uniform support scheme, the overall stability of the roof in the stress concentration zone is relatively good. However, the plastic zones in the two ribs, shoulder corners, and floor corners are extensive beneath the coal pillar, and local sustained shear failure still occurs. This indicates that the original support scheme is unable to accommodate the deformation and failure characteristics of the surrounding rock under a high-stress environment. To address this problem, an optimized support scheme was proposed.

In the optimized scheme, the bolt spacing was adjusted to 700 mm while the row spacing remained unchanged, and one additional bolt was installed in each rib. The roof bolts were kept unchanged from the original configuration. The cable arrangement was modified to a symmetrical layout, with one additional cable installed at the roof center. The spacing and row spacing of the cables remained unchanged, while the cable length was increased to 9200 mm. The cables were arranged at equal distances on both sides of the roadway centerline. The support layout of the optimized scheme is shown in Fig. 12, and the comparison between the optimized support parameters and those of the original support is presented in Table 3.

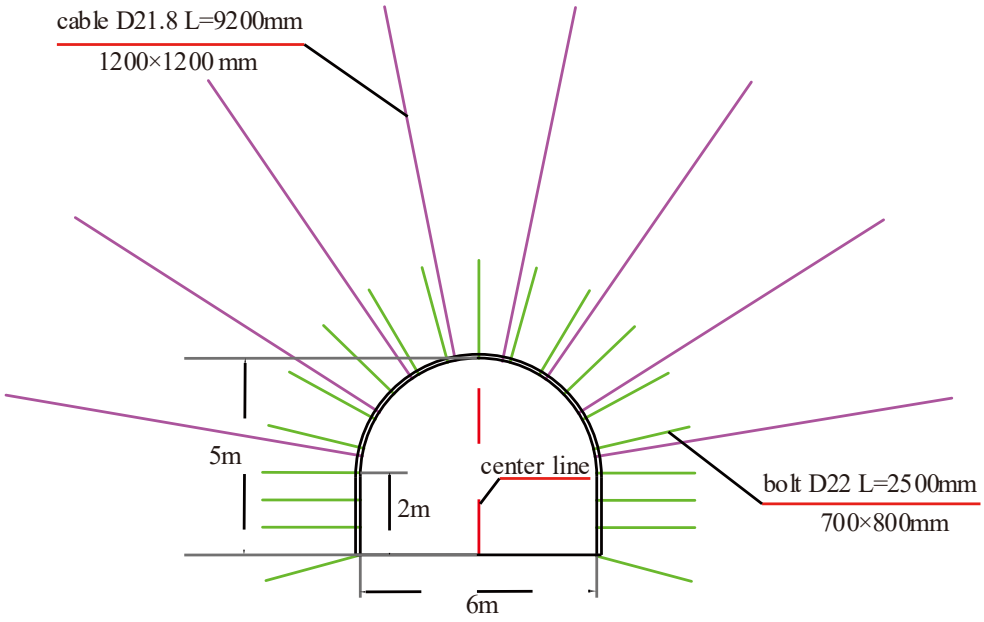


Figure 12. Cross-Section of the Optimized Roadway Support.

Support Scheme	Section Size / m	Number of Bolts	Number of Cables	Cable Specification / mm	Bolt Specification / mm	Cable Spacing and Row Spacing / mm	Bolt Spacing and Row Spacing / mm
Original Support	6×5	17	5	D21.8 L=7200	D22 L=2500	1200×1200	800×800
Optimized Support	6×5	19	6	D21.8 L=9200	D22 L=2500	1200×1200	700×800

Table 3. Comparison of Roadway Support Parameters between the Original and Optimized Schemes.

To verify the rationality of the optimized support scheme, numerical simulations were carried out in the stress concentration zone, i.e., within 40 – 80 m in horizontal distance from the stopping line, while maintaining the original roadway cross-sectional geometry.

The simulated vertical stress contours of the roadway surrounding rock are shown in Fig. 9. Compared with the pre-optimization condition, the vertical stress distribution of the surrounding rock at the (y=-60) m section is significantly improved after support optimization. The extent of the low-stress zones on the two ribs is markedly reduced, the stress concentration at the shoulder corners is effectively alleviated, and the stress contours in the roof become more uniformly distributed. In addition, the stress gradient in the surrounding rock decreases considerably, indicating that the optimized support enhances the load-bearing capacity of the shallow surrounding rock and promotes a more uniform transfer of stress into the deeper strata. Meanwhile, the morphology of the high-stress zone in the floor becomes more regular, the degree of stress concentration is slightly reduced, and the continuity and uniformity of the overall stress field are improved. Therefore, the optimized support can effectively suppress abnormal stress concentration in the surrounding rock after roadway excavation, improve the stress state of the surrounding rock, and enhance the overall stability of the roadway surrounding rock, thereby providing favorable mechanical conditions for the long-term safe service of the roadway.

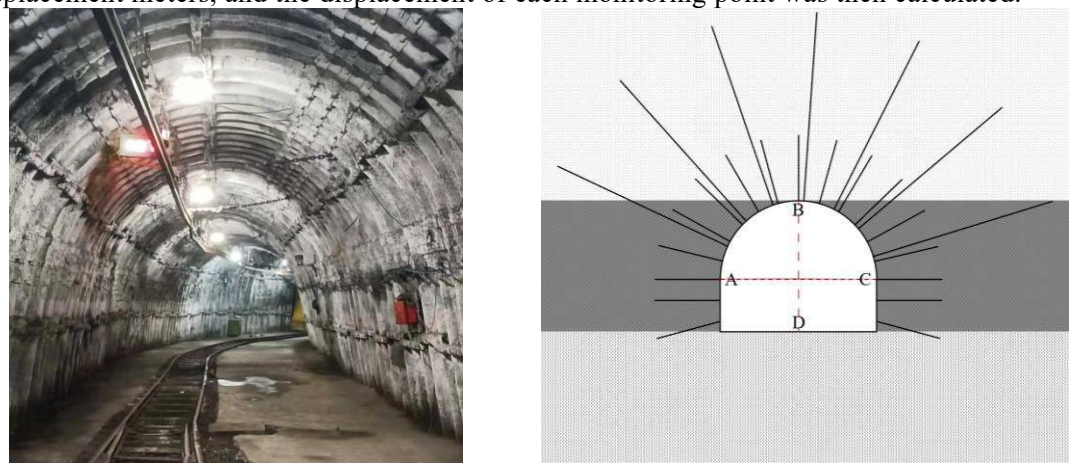
The plastic zone is shown in Fig. 10. A comparison of the plastic zone distribution at the (y=-60) m section before and after optimization shows that the extent of the plastic zone in the roadway surrounding rock is significantly reduced after support optimization. Plastic

failure is mainly concentrated in the shallow parts of the two ribs and in local floor-corner areas, while the original shear plastic zones extending from the ribs into the deeper surrounding rock are effectively restrained. The plastic zone distributions on the left and right ribs also become more symmetrical. At the same time, tensile failure and shear–tensile composite failure are significantly reduced, and the continuity of the plastic zone decreases markedly. These results indicate that the optimized support enhances the overall confinement capacity of the shallow surrounding rock, improves the cooperative load-bearing performance between the surrounding rock and the support structure, and restricts further expansion of the plastic zone into the deeper strata, thereby effectively improving the stability of the roadway surrounding rock under the high-stress influence of the coal pillar. Overall, the optimized support can significantly reduce the degree of plastic failure in the surrounding rock of the roadway beneath the coal pillar and provide reliable support for the safe and stable service of the roadway.

5. Field Engineering Verification

5.1 Roadway Surrounding Rock Deformation Monitoring

In the stress concentration zone of the west-wing auxiliary haulage roadway, the section located −60 to −40 m from the stopping line of the 110501 working face was selected as the test section. Monitoring points were arranged to measure the deformation of the roadway surrounding rock, and the support performance before and after optimization was compared. Displacement monitoring devices were installed on the roadway surface using the cross-point layout method, and the specific working principle is shown in Fig. 13(b). At fixed time intervals, the distances between monitoring points AC and BD were measured using displacement meters, and the displacement of each monitoring point was then calculated.



(a) Field layout; (b) Cross-measurement method

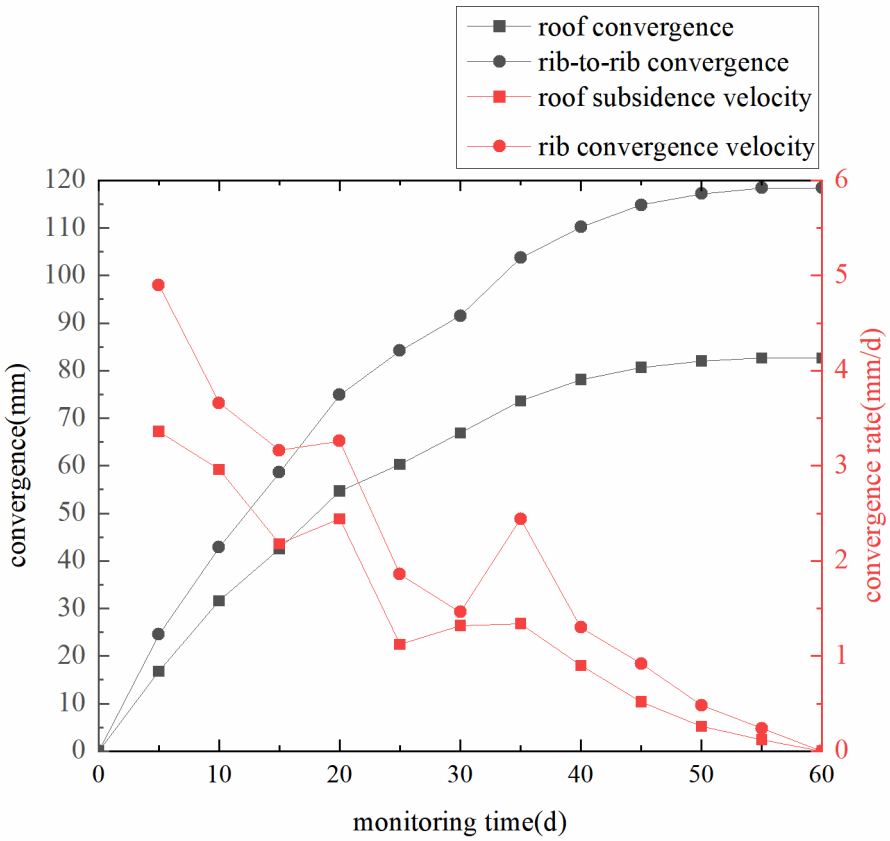
Figure 13. Field monitoring arrangement.

Fig. 14 presents the monitoring results of roadway surrounding rock displacement under the two different support schemes. The monitoring results show that under the original support scheme, the final roof-to-floor convergence and rib-to-rib convergence are 82.6 mm and 118.4 mm, respectively, whereas after optimization they decrease to 58.0 mm and 86.0 mm, corresponding to reductions of 29.78% and 27.36%, respectively. The optimized support shows a slightly better control effect on roof deformation.

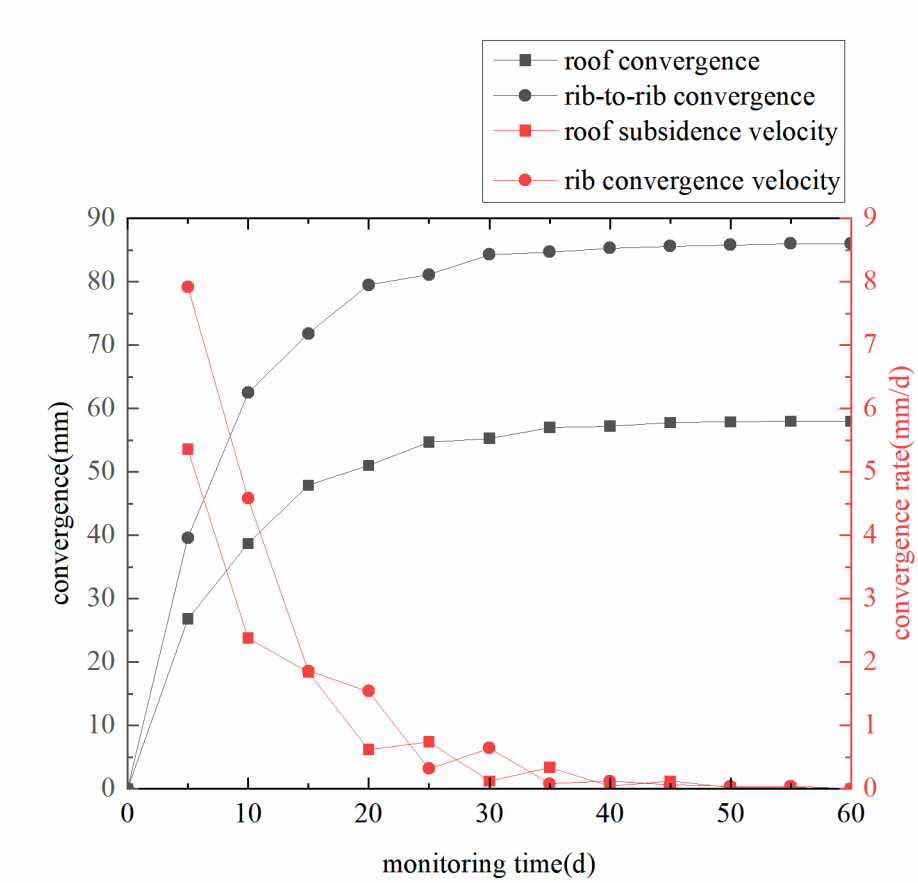
Under the original support scheme, the deformation of the surrounding rock lasts for a relatively long period. At 30 days, the roof-to-floor convergence and rib-to-rib convergence account for only 80.99% and 77.28% of their final values, respectively. The convergence rate attenuates slowly, and obvious fluctuations occur during 30–35 days. The surrounding rock does not tend to stabilize until approximately 45 days, and the additional convergence during 30–60 days still reaches 15.7 mm and 26.9 mm, respectively.

After support optimization, the deformation is mainly concentrated in the early rapid-release stage. Although the initial convergence rate is higher than that under the original scheme, the rate attenuates much more rapidly. At 30 days, the convergence accounts for more than 95% of the final value, and the stabilization time is advanced from approximately 45 days to about 30 days. During 35–60 days, the average convergence rates of the roof-to-floor and rib-to-rib deformation are only 0.04 mm/d and 0.05 mm/d, respectively, indicating that the later-stage deformation has basically converged and that the support system and surrounding rock have formed a stable cooperative load-bearing structure.

These results indicate that the optimized support scheme effectively suppresses the growth of rib displacement, improves the stress state of the surrounding rock, promotes the rapid formation of a stable load-bearing system, and significantly enhances roadway stability.



(a) Before support optimization



(b) After support optimization

Figure 14. Comparison of the Displacement and Displacement Rate of the Roof and Two Ribs before and after Support Optimization.

5.2 Roadway Roof Separation Monitoring

To accurately capture the movement characteristics of the overlying strata, such as bending subsidence and roof separation, roof separation indicators were installed at the preset monitoring points in the field. Through continuous monitoring and data analysis of roof separation on both sides of the roadway roof, the control effect of the support scheme on the roadway surrounding rock was quantitatively evaluated, thereby enabling dynamic tracking of the movement behavior of the overlying strata.

The roof separation indicators adopted a dual-base-point design, including a shallow base point and a deep base point. The anchorage depth of the shallow base point was 2.5 m, while the deep base point extended to a depth of 10 m. The monitoring results are shown in Fig. 15. The roof separation before and after support optimization exhibits a similar evolution pattern, characterized by slow growth in the early stage, staged abrupt increases in the middle stage, and gradual stabilization in the later stage. The periods of 15–20 days and 30–35 days correspond to the stages with pronounced abrupt increases, while the separation tends to stabilize after 50 days.

For the shallow base point, the final roof separation under the original support scheme is 9.2 mm, which decreases to 7.8 mm after optimization, corresponding to a reduction of 15.22%. During the abrupt-increase stage of 15–20 days, the separation increment decreases from 2.0 mm to 1.7 mm, and during the 30–35 days stage, it decreases from 1.8 mm to 1.5 mm. For the deep base point, the final roof separation decreases from 24.4 mm under the original support scheme to 22.9 mm after optimization, corresponding to a reduction of 6.15%. The separation increment during 15–20 days decreases from 5.5 mm to 5.1 mm, and that during 30–35 days decreases from 4.8 mm to 4.6 mm. In the stable stage, the roof separations at the

shallow and deep base points are 9.2 mm and 24.4 mm under the original support scheme, respectively, and decrease to 7.8 mm and 22.9 mm after optimization.

Overall, the optimized support scheme shows a significant control effect on shallow roof separation. It enhances the anchorage-bearing capacity of the shallow roof strata, restrains crack propagation, significantly improves the development of roof separation, and effectively enhances the overall stability of the surrounding rock.

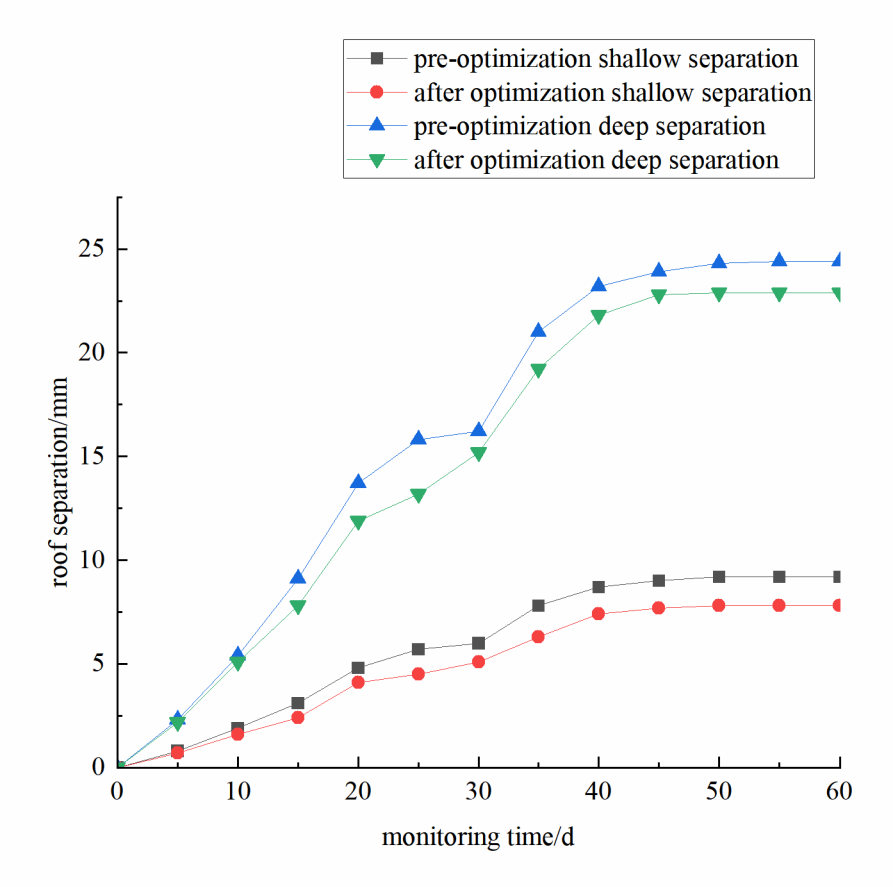


Figure 15. Variation in Roof Separation before and after Support Optimization.

6. Conclusions

(1) A calculation model for the mining-induced floor failure depth of the 110501 working face was established based on the plastic slip-line field theory. By incorporating the in situ mechanical parameters of the coal and rock masses, the maximum floor failure depth was determined to be approximately 22 m, which is basically consistent with the floor plastic yielding range obtained from numerical simulation. The plastic zone in the goaf floor generally presents a bowl-shaped distribution, and the failure mechanism exhibits a progressive evolution from shallow tensile failure to deep shear-slip failure, indicating that mining-induced stress has a significant deep transfer effect in the floor rock mass. Considering the floor failure depth and stress attenuation characteristics, it is reasonable to arrange the west-wing auxiliary haulage roadway in the rock strata 40 m below the floor of the goaf of the 110501 working face.

(2) After mining of the 110501 working face, the vertical stress in the underlying strata shows a spatial distribution pattern characterized by pressure relief in the central goaf region and stress concentration near the stopping line and coal pillar side. With the advancement of the working face, the mining-induced high-stress zone gradually migrates toward the goaf boundary and the stopping-line coal pillar side. The maximum vertical stress increases from 24.940 MPa to 34.596 MPa, corresponding to an increase of approximately 38.7%. The floor stress beneath the stopping-line coal pillar exhibits an obvious depth-dependent effect. The shallow strata show higher stress peaks and larger stress gradients, whereas the stress peaks in the deeper strata gradually attenuate and become smoother. This indicates that the

concentrated load induced by the stopping-line coal pillar is the main factor controlling the stability of the surrounding rock of the underlying roadway.

(3) The stress distribution and plastic zone development of the surrounding rock of the west-wing auxiliary haulage roadway exhibit pronounced zonal characteristics along the excavation direction. In the coal-pillar influence zone, the peak vertical stress on the two ribs reaches 30.53 MPa, with a stress concentration factor of 1.74, and the plastic zones in the two ribs, shoulder corners, and floor corners are significantly developed. In the stopping-line transition zone, the stress state of the surrounding rock rapidly changes from a high-stress state to a pressure-relief state, accompanied by a large stress gradient. After entering the area beneath the goaf, the vertical stress of the surrounding rock decreases significantly, and the plastic zone contracts markedly. Overall, the roadway failure degree follows the order of beneath the coal pillar > beneath the stopping line > beneath the goaf. The dominant failure mode is shear failure, while tensile-shear composite failure occurs locally in the floor corners and shallow floor strata.

(4) To address the insufficient control of the two ribs and shoulder corners in the high-stress zone affected by the coal pillar, a differentiated support scheme was proposed, with the main measures including increasing the density of rib bolts, adding additional rib bolts, optimizing the symmetrical arrangement of cables, and increasing the cable length. Numerical simulation results show that after support optimization, the stress distribution in the roadway surrounding rock becomes more uniform, the extent of the plastic zone is significantly reduced, and deep shear failure in the two ribs is effectively restrained. Field monitoring results show that the final roof-to-floor convergence and rib-to-rib convergence decrease from 82.6 mm and 118.4 mm to 58.0 mm and 86.0 mm, respectively. The roof separations at the shallow and deep base points are reduced by 15.22% and 6.15%, respectively. The optimized support scheme significantly improves the cooperative load-bearing capacity of the surrounding rock–support structure and can effectively ensure the long-term stability of the roadway in the stopping-line coal pillar influence zone.

Author contributions

Y.L.investigation, data curation,validation,writing—original draft. J.Y.: investigation, validation, writing—review and editing. S.D., X.Z., Y.F. and G.C.experiment data curation,validation.

Funding

(1) Anhui University of Science and Technology Scientific Research Start-up Fund for High-Level Talents (Grant No. 2023yjrc04), (2) Project supported by the Young Scientists Fund of the National Natural Science Foundation of China (Grant No.52304074).

Data availability

Some or all data, models, or codes generated or used during the study are available from the corresponding authors by request.

References

1. Kang, H. Support technologies for deep and complex roadways in underground coal mines: a review. International Journal of Coal Science & Technology 1, 261–277 (2014).
2. Xie, S. et al. Surrounding rock control mechanism of deep coal roadways and its application. International Journal of Mining Science and Technology 25, 429–434 (2015).
3. Wang, B. et al. Surrounding rock deformation and stress evolution in pre-driven longwall recovery rooms at the end of mining stage. International Journal of Coal Science & Technology 6, 536–546 (2019).
4. Kang, Q., He, F., Yin, S. & Yang, Y. Attenuation law of concentrated stress under coal pillar of close coal seams and its application. Scientific Reports 12, 21753 (2022).
5. Liu, H.-Q., Wang, L., Han, L.-C., Liu, P. & Zou, P. Study on the Instability Mechanism and Control Measures of a Roadway in a Mine with Retained Coal Pillars and Close Coal Seams. Shock and Vibration 2021, 8871807 (2021).

6. Wang, X.-H. et al. Selection and Optimization Mechanism of the Lower Return Roadway Layout in the near Residual Coal Pillar Area. Processes 10, 2471 (2022).
7. Wu, F. et al. Characteristics of Stress Field and Damage Law of Coal Rock in Residual Pillar of Top Slice and Its Application. Front. Earth Sci. 10, (2022).
8. Wang, X.-H. et al. Deformation and Failure Mechanism of the Lower Roadway in a Close-Range Residual Coal Pillar Area. Front. Earth Sci. 10, (2022).
9. Li, Y., Yao, Y., Zhu, T., Zeng, F. & Chang, G. Mechanical analysis and application of floor failure mechanism under repeated mining in close-distance coal seams. Sci Rep 16, 2728 (2025).
10. Liu, W., Han, M. & Zhao, J. Prediction of Floor Failure Depth Based on Dividing Deep and Shallow Mining for Risk Assessment of Mine Water Inrush. Water 16, 2786 (2024).
11. Kong, Z. et al. Theory and numerical simulation study on the plastic slip failure mechanism of multi-layered coal seam Floors-A case analysis. Front. Earth Sci. 13, (2025).
12. Yin, S., Zheng, X., Wang, E., Kang, Q. & Zhang, X. Non-uniform failure and differential pressure relief technology of roadway under irregular goafs in deep close-distance coal seams. Sci Rep 13, 18527 (2023).
13. Wang, C., Yao, H. & Huang, Y. Stability control of goaf-driven roadway surrounding rock under interchange remaining coal pillar in close distance coal seams. Energy Science & Engineering 12, 2553–2567 (2024).
14. Xia, Z. et al. Numerical study of stability of mining roadways with 6.0-m section coal pillars under influence of repeated mining. International Journal of Rock Mechanics and Mining Sciences 138, 104641 (2021).
15. Shang, Y. et al. Study on Failure Characteristics and Control Technology of Roadway Surrounding Rock under Repeated Mining in Close-Distance Coal Seam. Mathematics 10, 2166 (2022).
16. Xiang, Z. et al. Failure Characteristics and Stability Control of Bolt Support in Thick-Coal-Seam Roadway of Three Typical Coal Mines in China. Shock and Vibration 2021, 5589085 (2021).
17. Xie, X. et al. Deformation Mechanism and Control Technology of Surrounding Rock of Three-Soft Coal Roadways under High Horizontal Stress. Energies 16, 728 (2023).
18. Yao, W., Liu, G., Pang, J. & Huang, X. Instability Mechanism and Surrounding Rock Control Technology of Roadway Subjected to Mining Dynamic Loading with Short Distance: A Case Study of the Gubei Coal Mine in China. Geotech Geol Eng 41, 1407–1427 (2023).
19. Chen, D. et al. Failure mechanism and divisional differentiated control of surrounding rock in mining roadway under remaining coal pillar in close-distance coal seam. Energy Science & Engineering 11, 1412–1435 (2023).
20. Li, G., Wu, W., Cai, T. & Yang, Q. Study on optimizing the layout of lower coal seam roadways considering stress transmission in coal pillars. Results in Engineering 26, 105544 (2025).